Published in final edited form as:
Cell Host Microbe. 2011 December 15; 10(6): 563–576. doi:10.1016/j.chom.2011.10.014.

Adeno-Associated Virus 2 Infection Requires Endocytosis through the CLIC/GEEC Pathway

Mathieu Nonnenmacher[1] and **Thomas Weber**[1,*]
[1]Cardiovascular Research Center, Mount Sinai School of Medicine, New York, NY 10029, USA

SUMMARY

Adeno-associated viruses (AAVs) are non-pathogenic, non-enveloped, single-stranded DNA viruses in development as gene therapy vectors. AAV internalization was postulated to proceed via a dynamin-dependent endocytic mechanism. Revisiting this, we find that infectious endocytosis of the prototypical AAV, AAV2, is independent of clathrin, caveolin and dynamin. AAV2 infection is sensitive to EIPA, a fluid-phase uptake inhibitor, but is unaffected by Rac1 mutants or other macropinocytosis inhibitors. In contrast, AAV2 infection requires actin cytoskeleton remodeling and membrane cholesterol, and is sensitive to inhibition of Cdc42, Arf1 and GRAF1, factors known to be involved in the formation of clathrin-independent carriers (CLIC). AAV2 virions are internalized in the detergent-resistant GPI-anchored-protein-enriched endosomal compartment (GEEC) and translocated to the Golgi apparatus, similarly to the CLIC/GEEC marker cholera toxin B. Our results indicate that —unlike the viral entry mechanisms described so far— AAV2 uses the pleiomorphic CLIC/GEEC pathway as its major endocytic infection route.

Keywords

adeno-associated virus; AAV2; endocytosis; CLIC/GEEC; GRAF1; Cdc42; Arf1; dynamin

INTRODUCTION

Adeno-associated viruses (AAVs) are non-enveloped, single-stranded DNA viruses of the family *Parvoviridae* and the genus *Dependovirus* that are not associated with any known disease and show great potential as gene transfer vectors. AAVs depend on co-infection with a helper virus, such as adenovirus, herpesvirus or papillomavirus for productive replication (Grimm and Kay, 2003). So far, 13 distinct AAV serotypes and more than 100 variants isolated from primates have been described (Daya and Berns, 2008). The AAV serotypes show distinct transduction efficiencies and tissue tropism both *in vitro* and *in vivo*. This variability is in part a result of the diversity of AAV surface receptors, but other evidence suggests that the nature of the endocytic pathway taken by the virus is also critical for a successful transduction (Bhrigu and Trempe, 2009; Hansen et al., 2000).

*Correspondence: thomas.weber@mssm.edu.

SUPPLEMENTAL INFORMATION

Supplemental Information includes four figures, one table, Supplemental Experimental Procedures and Supplemental References and can be found online with this article at:

Several studies have suggested that recombinant AAV2 internalization proceeds via a dynamin-dependent mechanism (Bartlett et al., 2000; Duan et al., 1999) and, based on rapid uptake kinetics and partial co-localization with endocytosed transferrin, it was postulated that AAV2 is endocytosed via clathrin-coated vesicles. Interestingly, inhibition of dynamin could only partially block virus endocytosis, indicating that AAV2 can use alternative entry routes (Duan et al., 1999). Another study suggested that AAV2 internalization was dependent on the GTPase Rac1 (Sanlioglu et al., 2000), which is a major effector of macropinocytosis, a bulk fluid-phase endocytic mechanism that is independent of clathrin and dynamin (Doherty and McMahon, 2009).

Here we revisit the internalization mechanism of recombinant AAV2 vectors (rAAV2, herein referred to as AAV2) into highly permissive HeLa and HEK293T cells using methods specifically designed to minimize potential post-entry effects of pharmacological inhibitors or recombinant proteins. Because infection with wild-type AAV can be measured only in the presence of a helper virus, which would render the analysis of AAV2 endocytosis difficult—if not impossible—we use recombinant AAV2 carrying reporter genes instead of wild-type virus and use the terms infection and transduction interchangeably. We found that AAV2 infection occurs independently of clathrin, caveolin and dynamin, and that AAV2 infection is sensitive to the amiloride derivative EIPA but does not display other characteristics of macropinocytosis. In contrast, infectious entry of AAV2 is dependent on an intact actin cytoskeleton and membrane cholesterol and is sensitive to inhibition of the three main effectors of the clathrin-independent carriers/GPI-anchored-protein-enriched endosomal compartment (CLIC/GEEC) pathway—namely GRAF1 (Lundmark et al., 2008), Cdc42 (Sabharanjak et al., 2002) and Arf1 (Kumari and Mayor, 2008). AAV2 co-localizes with internalized GPI-GFP and cholera toxin B subunit (CtxB) in early endosomal vesicles and is subsequently transported to the Golgi apparatus together with CtxB. Interestingly, a fraction of AAV2 is internalized via a dynamin-dependent pathway, but this population does not play a major role in infection. Taken together, our results indicate that—unlike any other virus studied so far—AAV2 uses the CLIC/GEEC endocytic pathway as a major infectious entry route.

RESULTS

AAV2 Infection Is Independent of Clathrin, Caveolin and Dynamin

AAVs contain a single-stranded DNA genome and require conversion to double-stranded DNA for gene expression. This essential step is rate-limiting and can be influenced by genomic stress and other undefined factors (Ferrari et al., 1996). To rule out any potential effect of pharmacological inhibitors or ectopic protein expression on viral DNA second-strand synthesis, we used a recombinant AAV2 carrying a self-complementary mCherry cassette. This AAV vector does not depend on complementary strand synthesis for transgene expression (Wang et al., 2003). For some experiments we used a recombinant AAV2 carrying a single-stranded luciferase cassette. These vectors are referred to as AAV2-cherry and AAV2-luc respectively.

We first investigated whether clathrin- or caveolae-mediated endocytosis is involved in AAV2 transduction. Clathrin-mediated endocytosis can be blocked by overexpression of a truncation mutant of Eps15, a component of clathrin-coated vesicles (Benmerah et al., 1999). As shown in Figure 1A, AAV2-cherry transduction—measured by flow cytometry—was completely unaffected by expression of GFP-tagged Eps15Δ95/295 (Eps15DN), whereas transferrin internalization was dramatically decreased. To confirm independently that AAV2 transduction is not dependent on clathrin-mediated endocytosis, cells were infected in the presence of chlorpromazine, a known inhibitor of clathrin-coated pit assembly (Wang et al., 1993). Chlorpromazine treatment did not reduce AAV2 transduction

of HeLa cells, while transferrin uptake was inhibited by approximately 75% under the same conditions (Figure 1B). To minimize drug toxicity and to prevent pleiotropic effects on post-entry steps of infection (e.g., endosomal escape or viral DNA synthesis), the virus was stripped from the cell surface by heparin treatment 30 minutes after the onset of endocytosis, and cells were then incubated overnight in drug-free medium to allow transgene expression. This procedure, which allows the removal of up to 99% of surface-bound AAV2 (Figure S1), was used in all our studies involving pharmacological inhibitors. Under the conditions used, none of our inhibitors caused significant toxicity.

Next, we investigated the role of caveolae-mediated endocytosis in AAV2 transduction. To block caveolar endocytosis, we expressed caveolin-1 N-terminally fused to EGFP (Cav1DN), known to act as a dominant-negative mutant (Pelkmans et al., 2001). Cav1DN expression reduced the uptake of CtxB, a marker of caveolar endocytosis (Parton et al., 1994), by ~50%, but did not affect AAV2 transduction (Figure 1C). Clathrin- and caveolae-mediated endocytosis are both dynamin-dependent, but dynamin is also involved in phagocytosis, flotillin-dependent endocytosis and interleukin receptor 2-β endocytosis (Doherty and McMahon, 2009). Hence, we re-investigated the role of dynamin in AAV2 transduction. Inhibition of dynamin-2 function by the dominant-negative mutant Dyn2K44A efficiently blocked transferrin endocytosis but had little or no effect on AAV2 transduction in either HeLa or 293T cells, (Figure 1D): Instead, AAV2 transduction was slightly increased in 293T cells expressing Dyn2K44A (+25%, Figure 1D). We also investigated the effect of dynasore, a potent and reversible dynamin inhibitor (Macia et al., 2006). We observed an almost complete inhibition of transferrin uptake in HeLa cells treated with 80 μM dynasore (Figure 1E), while AAV2 uptake was unchanged in 293T cells and only moderately affected in HeLa cells under the same conditions (Figure 1E). Strikingly, dynasore had no effect on AAV2 transduction in HeLa cells and stimulated (+60%) transduction in 293T cells (Figure 1F). In contrast, infection of HeLa cells by a recombinant adenovirus type 5 vector carrying a luciferase transgene (Ad5-Luc) was reduced by 65–70% following dynasore treatment (Figure 1G), which is consistent with previous studies showing that Ad5 entry occurs in clathrin-coated pits and requires dynamin (Meier and Greber, 2003). Together, these data demonstrate that although dynamin may contribute to AAV2 internalization to some extent, it is not strictly required for AAV2 infection.

AAV2 Infection Is Sensitive to EIPA but Does Not Involve Macropinocytosis

The above findings indicate that the infectious entry of AAV2 occurs mainly through a dynamin-independent pathway. Previous studies reported that AAV2 endocytosis is Rac1-dependent (Sanlioglu et al., 2000), which would be consistent with AAV2 being endocytosed by macropinocytosis, a dynamin-independent endocytic mechanism mediating fluid-phase uptake (Ridley and Hall, 1992). Expression of the dominant-negative mutant Rac1T17N (Rac1DN) efficiently blocked internalization of 70 kDa dextran, a fluid-phase marker specific for macropinocytosis, but showed little effect on AAV2 uptake in HeLa cells (Figure 2A). Similarly, inhibition of Rac1 did not significantly reduce transduction by AAV2-cherry or AAV2-Luc in 293T cells but dramatically blocked transduction by Ad5 vectors (Figure 2B, C), which was expected since Ad5 internalization is Rac1-dependent (Meier and Greber, 2003). Flow cytometry confirmed these results; no significant inhibition of AAV2 transduction by Rac1DN in either HeLa or 293T cells was observed (Figure 2D), whereas constitutively active Rac1 (Rac1Q61L) slightly decreased transduction in both cell lines. We also tested several chemical inhibitors of macropinocytosis: 5-(N-Ethyl-N-isopropyl) amiloride (EIPA), an inhibitor of Na^+/H^+ exchange, LY294002, a phosphoinositide-3 kinase (PI3K) inhibitor, IPA-3, a Pak1 inhibitor and EHT1864, a Rac1 inhibitor. Only EIPA inhibited AAV2 transduction (Figure 2E, left panel), whereas all compounds efficiently blocked macropinocytic uptake of 70 kDa dextran (Figure 2E, right

panel). EIPA reduced AAV2 entry by 50% in 293T cells but not in HeLa cells (Figure 2F). A hallmark of viruses that are internalized by macropinocytosis or other Rac1-dependent mechanisms is that they trigger a robust increase of fluid-phase uptake (Mercer and Helenius, 2009). In HeLa cells, 70 kDa dextran uptake was strongly enhanced by incubation with Ad5 at a MOI of 10^5 virions/cell (5-fold) and by PMA (3-fold), a phorbol ester known to increase macropinocytosis (Swanson, 1989) but was not affected by incubation with high amounts of AAV2 (10^5 genome-containing particles (gcp) per cell; Figure 2G). Similarly, 293T cells exposed to AAV2 did not internalize the fluid-phase markers 70 kDa dextran, 10 kDa dextran or Lucifer yellow more efficiently than uninfected control cells (Figure 2H). Overall, these results indicate that while AAV2 infection is EIPA-sensitive, it does not occur via macropinocytosis.

AAV2 Infection Is Dependent on Actin and Cholesterol

Several dynamin-independent endocytic mechanisms involve actin cytoskeleton dynamics and cholesterol-rich detergent-resistant microdomains in order to alter plasma membrane morphology or trigger vesicle scission (Doherty and McMahon, 2009). Exposure of HeLa cells to high titers of AAV2 (10^5 gcp/cell) induced extensive remodeling of the plasma membrane, including blebbing and filopodia extension (Figure 3A, left panels) as well as profound modifications of the actin cytoskeleton, as shown by phalloidin staining (Figure 3A, right panels). When actin polymerization or depolymerization was prevented by treatment with cytochalasin D and jasplakinolide respectively, we observed a significant decrease in AAV2 endocytosis and transduction in both HeLa and 293T cells, whereas virus binding was unaffected or enhanced (Figure 3B). We next sought to determine whether membrane cholesterol and lipid raft microdomains are necessary for AAV2 infection. Most internalized AAV2 was resistant to cold triton extraction on live cells, while fluorescent transferrin was almost completely extracted (Figure 3C), which strongly suggests that internalized AAV2 particles are associated with cholesterol-rich detergent-resistant membranes (DRMs). Consistently, in sucrose density gradients with triton cell lysates AAV2 was mostly recovered from the low-density fractions enriched in the lipid raft marker flotillin-1. In contrast, transferrin and adenovirus 5 sedimented in triton-soluble fractions, which is consistent with internalization in vesicles derived from clathrin-coated pits (Figure 3D). As expected for a lipid-raft-dependent pathway, AAV2 transduction and internalization were significantly reduced in HeLa cells treated with methyl-β-cyclodextrin or filipin III (Figure 3E). These studies could not be extended to 293T cells because both drugs induced rapid cell detachment, but the cholesterol synthesis inhibitor pravastatin reduced infection by 40% in both cell lines (data not shown). Overall, these results show that both actin and membrane cholesterol are necessary for AAV2 uptake and that AAV2 virions are internalized into a detergent-resistant endocytic compartment.

AAV2 Infection Involves Effectors of the CLIC/GEEC Pathway

The above results indicate that AAV2 infectious entry is mostly independent of dynamin and macropinocytosis and requires actin and cholesterol microdomains. These features are reminiscent of the recently characterized CLIC/GEEC pathway, which mediates uptake of GPI-anchored proteins, fluid-phase markers and CtxB (Doherty and McMahon, 2009). CLIC/GEEC endocytosis is regulated by Arf1 and Cdc42 GTPases (Chadda et al., 2007; Kumari and Mayor, 2008), which promote membrane curvature and local actin polymerization, respectively. CLIC/GEEC endocytosis is also critically dependent on the Rho GTPase-activating protein GRAF1 (GTPase Regulator Associated with Focal Adhesion Kinase) for the tubulation and scission of CLIC vesicles (Doherty and Lundmark, 2009; Lundmark et al., 2008). We first investigated the role of Arf1 and Cdc42 proteins in AAV2 transduction and entry. Dominant-negative mutants of Arf1 (Arf1T31N) and Cdc42 (Cdc42T17N) significantly reduced AAV2-cherry transduction in both HeLa and 293T cells,

as measured by flow cytometry (Figure 4A, B). Interestingly, the constitutively active form of Arf1 (Arf1Q71L) also blocked AAV2 transduction, whereas constitutively active Cdc42 (Cdc42G12V) had no effect (Figure 4A, B). AAV2-luc transduction of 293T cells was also reduced by 60% and 70% in 293T cells expressing Cdc42DN or Arf1DN respectively (Figure 4C). Both Arf1DN and Cdc42DN inhibited AAV2 uptake (70% reduction; Figure 4D), which strongly suggests that both proteins are directly involved in viral entry. Subcellular localization analysis using GFP-tagged Cdc42 showed that a large proportion of incoming AAV2 virions (40% to 50% pixel overlap) co-localize with Cdc42-positive peripheral endocytic structures at early time points (Figure 4E, left panel). At later time points (40 min), co-localization could still be observed to some extent (~30% overlap), mostly in perinuclear structures. In contrast, Ad5 virions showed no significant overlap with Cdc42-labeled structures (Figure 4E). Cdc42 activity is blocked by amiloride (Koivusalo et al., 2010). Because we previously observed that the amiloride-derivative EIPA inhibits AAV2 transduction (Figure 2E), we investigated the effect of EIPA on the internalization of cholera toxin B, which is internalized via both CLIC endosomes and caveolae (Howes et al., 2010; Kirkham et al., 2005; Sabharanjak et al., 2002). EIPA reduced CtxB endocytosis by 50% in HeLa cells, and CtxB that was internalized in the presence of EIPA was restricted to peripheral vesicles instead of being transported to the perinuclear area (Figure 4F, G). Strikingly, inhibition of caveolar endocytosis by dynasore did not affect CtxB uptake, but simultaneous treatment with both dynasore and EIPA almost completely abolished CtxB internalization (Figure 4F, G), which is consistent with EIPA being a potent inhibitor of CLIC/GEEC endocytosis. Similarly, EIPA and dynasore showed a strong synergistic effect on AAV2 transduction and endocytosis (Figure 4H), which suggests: 1) that AAV2 can enter cells via two distinct endocytic pathways, Dynamin-dependent endocytosis and CLIC/GEEC endocytosis; and 2) that only CLIC/GEEC endocytosis leads to efficient infection.

We next investigated the role of GRAF1 in AAV2 infection. Ectopic expression of the dominant negative truncation mutant GRAF1Δ384-814 (Lundmark et al., 2008) led to a 30% and 60% reduction in AAV2-cherry transduction in HeLa and 293T cells, respectively (Figure 5A). GRAF1DN expression also reduced AAV2-Luc transgene expression in 293T cells but conversely increased Ad5-Luc transduction by 2-fold (Figure 5B), showing that GRAF1DN selectively modulates the AAV2 infectious pathway. GRAF1DN expression also inhibited AAV2 uptake in 293T cells (60% inhibition), which confirms that GRAF1 directly regulates AAV2 endocytosis (Figure 5C). To confirm further the role of GRAF1 in AAV2 infection, we depleted endogenous GRAF1 with small interfering RNA (siRNA). Transfection with two distinct siRNAs (Lundmark et al., 2008) efficiently reduced GRAF1 expression in HeLa and 293T cells (Figure S2) and dramatically decreased AAV2 transduction (Figure 5D, E). Again, GRAF1 knock-down specifically modulated the AAV2 infectious pathway, since Ad5 transduction was not decreased in GRAF1-depleted cells (Figure 5F). GRAF1 knockdown efficiently inhibited AAV2 entry in 293T cells (50% reduction) and to a lesser extent in HeLa cells (20% reduction; Figure 5G). This effect was greatly enhanced by dynasore treatment in both cell types (80% reduction), confirming the existence of two AAV2 endocytic pathways that are dependent on GRAF1 and dynamin, respectively. At early time points, confocal microscopy showed extensive co-localization of GFP-GRAF1 with internalized AAV2 virions (>47% overlap), but not with Ad5 virions (0.9%). As observed with Cdc42, the extent of co-localization diminished rapidly, since only 20% overlap was observed 40 minutes after the onset of AAV2 endocytosis (Figure 5H). Overall, the data indicate that AAV2 infectious entry occurs via CLIC/GEEC endocytosis, although a fraction of virions are internalized through dynamin-dependent endocytosis, which does not result in efficient infection.

AAV2 Internalization and Trafficking via CLIC/GEEC Endosomes

We next investigated whether internalized AAV2 virions accumulate in the same endosomal structures as the prototypical CLIC cargos, CtxB and GPI-anchored proteins. AAV2 co-localized to a large extent with CtxB (Figure 6A, B) and internalized glycosylphosphatidyl-inositol (GPI)-anchored GFP (Figure 6C), labeled with a fluorescent anti-GFP antibody (Figure 6C). Co-localization with CtxB and GFP-GPI was stable over time (Figure 6A-C), which suggests that AAV2 follows the same trafficking route as CtxB and GFP-GPI from the plasma membrane to the perinuclear region. Consistently, AAV2 virions, but not Ad5 virions, could be recovered from GPI- and GRAF1-positive membranes purified by immunoisolation with an anti-GFP antibody (Figure 6D). In sucrose gradients, both GFP-GRAF1 and GFP-GPI were highly enriched in the same low-density fractions as AAV2 (Figure 6E), and GFP-GRAF1 immunoisolation performed on pooled DRM fractions confirmed that AAV2 particles were physically associated with GRAF1-enriched vesicles in lipid rafts (Figure 6F).

The GEEC pathway involves rapid acidification of endocytic vacuoles (Kalia et al., 2006), so we evaluated the impact of modifying the endosomal pH on AAV2 transduction. As previously reported (Bartlett et al., 2000; Douar et al., 2001), bafilomycin A1, an inhibitor of endosome acidification, completely blocked AAV2 transduction when the drug was added within 1 hr after the onset of endocytosis (Figure S3). Consistent with previous studies (Johnson et al., 2010; Pajusola et al., 2002), AAV2 virions rapidly trafficked to the Golgi apparatus, showing >30% co-localization with the Golgi marker giantin 2 hours post-infection (Figure 7A, B). Brefeldin A, a drug causing Golgi disassembly, dramatically inhibited AAV2 transduction (Figure 7C). These results are consistent with a role for Golgi transport in AAV2 infection, although we can not exclude other effects of brefeldin A on different parts of the endosomal system. AAV2 trafficking to the Golgi was unaffected in cells treated with dynasore but was reduced more than 10-fold following EIPA treatment (Figure 7D). Similarly, AAV2 transport to the Golgi was strongly impaired in cells overexpressing dominant negative mutants of GRAF1 (6-fold), Cdc42 (10-fold) or Arf1 (7-fold) (Figure 7D).

Taken together, our findings indicate that AAV2 internalization into CLIC/GEEC endosomes is necessary for efficient trafficking and infection.

DISCUSSION

In this report, we demonstrate that AAV2 infectious entry in HeLa and 293T cells has all the hallmarks of CLIC/GEEC endocytosis: It is functionally dependent of GRAF1, Cdc42, Arf1, the actin cytoskeleton and membrane cholesterol, and internalized virions accumulate in endocytic vesicles enriched in CLIC/GEEC markers such as CtxB, GPI-anchored proteins, and GRAF1. AAV2 is unique in its ability to use the CLIC/GEEC pathway as a route of infectious entry. We found that AAV2 transduction does not require clathrin, caveolin or dynamin, which was unexpected because previous reports suggested that inhibition of dynamin reduces viral transduction by approximately 50% (Bartlett et al., 2000; Duan et al., 1999; Ren et al., 2007). Notably, these experiments relied on adenoviral vectors for overexpression of dominant negative dynamin (dynamin K44A), and it is now well established that adenovirus or adenoviral vectors induce dramatic changes in cell homeostasis that may profoundly affect AAV2 trafficking (Johnson et al., 2010; Xiao et al., 2002).

AAV2 infectious entry is sensitive to EIPA but does not depend on macropinocytosis. EIPA reduced CtxB uptake, and this effect was drastically increased when caveolar uptake of CtxB was blocked by dynamin inhibition. These results are in agreement with recent reports

showing that amiloride inhibits Cdc42 activity (Koivusalo et al., 2010) and, hence, likely reduces constitutive endocytosis of GPI-anchored proteins (Cortese et al., 2008; Tkachenko et al., 2004) through the CLIC/GEEC pathway. Inhibition of both CLIC/GEEC- and dynamin-dependent endocytosis was required to block completely AAV2 entry (Figure 4), which indicates that AAV2 can enter cells simultaneously via dynamin-dependent and -independent mechanisms. Our results indicate that the route of AAV2 endocytosis determines the fate of internalized virions and the efficiency of infection; apparently only CLIC/GEEC-mediated entry leads to efficient transduction, presumably due to increased trafficking of AAV2 virions to the Golgi apparatus (Figure 7). The retrograde transport mechanism leading to Golgi accumulation of AAV2 is largely unknown. We did not observe extensive virion accumulation in early, late or recycling endosomes labeled with Rab5, Rab7 or Rab11, respectively (data not shown), suggesting that AAV2 might bypass the classical endosomal system to reach the Golgi apparatus; although we can not rigorously exclude a role of these proteins in AAV infection, even in the absence of significant co-localization. In contrast, AAV2 and CtxB accumulated in the same transport intermediates from the plasma membrane to the Golgi (Figure 6A), which is reminiscent of previous studies showing that GPI-anchored proteins and CtxB are transported to the Golgi in carriers devoid of classical endosome markers (Nichols, 2002; Nichols et al., 2001).

Interestingly, a recent high-throughput siRNA study performed on human aortic endothelial cells showed that AAV2 transduction was strongly inhibited (from 3- to 15-fold) following siRNA knock-down of GRAF1, Arf1 or ARHGAP10, another CLIC/GEEC effector (Wallen et al., 2011). These observations suggest that our findings are likely valid in other cell types, including primary cells. To our knowledge, virus entry via CLIC/GEEC endocytosis has not been described so far. However, the characterization of other viral endocytic pathways has shown that viruses are able to take advantage of every available cellular internalization mechanism (Sieczkarski and Whittaker, 2002) and that they frequently use more than one route. The CLIC/GEEC system is a high-capacity, constitutive and pleiotropic endocytic mechanism that can lead to the internalization of the complete plasma membrane of a fibroblast in about 15 min (Howes et al., 2010). Thus, clathrin-independent carriers may constitute an attractive and potent entry mechanism for viruses and other pathogens. In addition, CLIC endosomes are highly acidic (Kalia et al., 2006) which creates a favorable environment for capsid or envelope modifications necessary for subsequent trafficking/sorting steps of many viruses, including AAV2 (Figure S3 and Bartlett et al., 2000). Intriguingly, several viruses show similarities with AAV2 in their mode of entry. Human papillomavirus type 16, lymphocytic choriomeningitis virus, and influenza virus have all been associated with endocytic mechanisms independent of clathrin, caveolin or macropinocytosis (Mercer et al., 2010), and simian virus 40 (SV40) can use a cholesterol-dependent, dynamin-independent pathway (Damm et al., 2005). In *Cav1*$^{-/-}$ cells SV40 internalization occurs in non-coated tubular vesicles (Ewers et al., 2009) similar to those formed by GRAF1 *in vitro* and *in vivo* (Lundmark et al., 2008). Other viruses have been documented to bind to GPI-anchored proteins as their attachment receptors, such as enterovirus 70 and echovirus with the decay-accelerating factor (Lakhan et al., 2009). In light of our results, it will be interesting to investigate whether the CLIC/GEEC pathway is a more general mode of viral endocytosis.

EXPERIMENTAL PROCEDURES

Materials

All commercially available reagents, plasmids and the sequences of primers and siRNAs used in this study are described in Supplemental Information.

Cells, Transfection, siRNA and Viruses

HEK293T and HeLa cells (ATCC, Manassas, VA) were maintained in DMEM with 10% FBS (Sigma, St Louis, MO), L-glutamine and antibiotics. 293T were transfected by calcium phosphate precipitation. HeLa cells were transfected with GeneJammer (Agilent, Santa Clara, CA) or Lipofectamine 2000 (Invitrogen, Carlsbad, CA). Stealth™ siRNAs (Table S1) were from Invitrogen and were transfected with Lipofectamine 2000. Recombinant AAV2 was produced and purified as previously described (Gigout et al., 2005; Grimm et al., 1998; Hirosue et al., 2007; Zolotukhin et al., 1999). Viral titers were determined by real-time PCR with transgene-specific primers (Table S1). Adenovirus type 5 (Ad5) vectors carrying the mCherry or luciferase transgene were kindly provided by Dr. Kleopatra Rapti and Dr. Lifang Lian (Mount Sinai School of Medicine, NY).

Viral Transduction Assays

For experiments involving chemical inhibitors, cells pretreated with inhibitors for 30 min were infected for 30–60 min at 37 °C with AAV2 or Ad5 carrying the mCherry or luciferase transgene. Surface AAV2 was stripped with 100 μg/ml heparin for 10 min in the presence of drugs. Ad5 was removed by acid wash in DMEM, 25 mM sodium acetate, pH 2.0 for 2 minutes on ice. Cells were then incubated overnight in drug-free medium. Luciferase activity was measured with Promega Luciferase Assay System in a Wallac luminometer (Perkin Elmer, San Jose, CA). Values were normalized to the total protein content of the lysates, measured by BCA assay. All pharmacological inhibitors were also tested with AAV2-cherry with similar results (data not shown). For experiments involving recombinant protein expression, cells were infected 24 hours post-transfection, incubated for 16–24 hr and assayed for fluorescence by flow cytometry or microscopy, or for luciferase activity.

Virus Binding and Endocytosis Assays

For binding studies, virus was added for 1 hr on ice before PBS wash. Cells were lysed in 1% NP-40 buffer, and DNA was extracted using Zyppy plasmid miniprep columns (Zymo Research, Orange, CA) with a 10 min incubation at 95 °C in lysis buffer to denature viral capsids. Viral DNA was quantified by real-time quantitative PCR (qPCR) using Clontech SYBR green mix with transgene-specific primers.

For AAV2 endocytosis studies, cells were infected for 1hr at 37 °C; then heparin was added for 10 min to remove surface-bound virus. Cells were trypsinized and low-molecular weight DNA was extracted. Viral genomes were quantified by qPCR with luciferase primers, and are referred to as “internalized AAV genomes”.

Endocytosis Assays with Endocytic Markers

Cells incubated on ice with fluorescent transferrin (20 μg/ml), cholera toxin (1 μg/ml), dextran (1 mg/ml), or lucifer yellow (1 mg/ml) were transferred to 37 °C for the indicated times. Endocytosis was stopped by ice-cold PBS washes, and surface-bound dyes were removed by acid treatment for 2 min on ice in DMEM, 25 mM sodium acetate, pH 2.0. Fluorescence was measured by microscopy as the average fluorescence of 3 different fields (approx. 200 cells per field) from 3 separate samples and quantified with Photoshop software (Adobe). For GPI internalization, cells expressing GFP-GPI were incubated with alexa555-conjugated anti-GFP antibody (1:400 dilution) on ice, washed and transferred to 37 °C. Surface-bound antibody could be stripped by removal of GFP-GPI with 0.5U of PI-PLC (Invitrogen) for 30 min at 4 °C (>95% surface fluorescence removal; data not shown). The anti-GFP antibody was highly specific since no labeling of untransfected neighboring cells was observed.

Immunofluorescence

HeLa cells plated on glass coverslips were fixed in 4% PFA in PBS for 15 min at room temperature, permeabilized with 0.2% triton X-100 and blocked for 1 hr with 0.5% BSA in PBS. For experiments using EIPA, cells were fixed in cold methanol for 5 min at −20 °C. After incubation with primary antibodies (overnight at 4 °C) and fluorescent secondary antibodies (1 hr at room temperature), nuclei were counterstained with DAPI and slides were mounted in Mowiol and observed with a Leica SP5 DM confocal microscope. All confocal images represent a single plane acquired with a 63x oil objective and a pinhole set at 1 Airy unit (optical slice ~0.8 μm). Quantification of co-localization was performed on three separate fields and at least two independent experiments using the Metamorph software.

Scanning Electron Microscopy

Cells grown on coverslips were incubated 1 hr on ice with ssLuc AAV2 (10^5 gcp/cell) and transferred to 37 °C for 10 min. Cells were fixed in 3% glutaraldehyde for 30 min, post-fixed in 1% OsO4 (4°C, 30 min), dehydrated in ethanol, critical point dried, coated with palladium-gold, and observed with a Hitachi S4300 field emission scanning electron microscope.

Triton Extraction, Cell Fractionation and Immunoisolation

Triton extraction of HeLa cells grown on coverslips was performed as previously described (Nichols et al., 2001) after infection with AAV2 (10^5 gcp/cell) for 30 min in the presence of fluorescent transferrin. For sucrose fractionation, cells grown in 150-mm plates were infected for 1 hr with AAV2 or Ad5 (10^4 gcp/cell). Biotinylated transferrin (5 μg/ml) was used as a marker of non-lipid raft membranes. Cell lysis and sucrose density gradient fractionation were performed as previously described (Legler et al., 2005). Viral DNA was extracted from each fraction with Zyppy columns and quantified by qPCR. For immunoisolation of GRAF1 and GFP-GPI containing membranes, 293T cells transfected with GFP-GPI or GFP-GRAF1 were lysed and scraped on ice in buffer containing 1% Triton X-100, 150 mM NaCl, 50mM Tris, pH 7.5 and protease inhibitors (2 ml buffer per 15-cm plate). Lysates were precleared 1 h at 4 °C with agarose-protein G beads (50 μl beads per 2-ml lysate) and incubated for 1h at 4 °C with 35 μl agarose-protein G beads coated with 2 μg anti-GFP antibody in lysis buffer with 1% BSA. Following extensive washes in lysis buffer/BSA, beads were suspended in PBS, and DNA was extracted with Zyppy columns. Normal mouse serum was used as immunoprecipitation control.

Statistical Analysis

Data are representative of at least three independent experiments, and values are given as mean of triplicates ± standard deviation (SD). Statistical significance is determined by paired Student's t-test. Only p-values ≤ 0.05 were considered statistically significant.

Supplementary Material

Refer to Web version on PubMed Central for supplementary material.

Acknowledgments

We gratefully acknowledge Alice Dautry (Institut Pasteur, Paris, France), Mark A. McNiven (Mayo Clinic, Rochester, MN, USA), Jürgen Kleinschmidt (Deutsches Krebsforschungszentrum, Heidelberg, Germany) and Sergei Zolotukhin (University of Florida, Gainesville, FL) for providing us with Eps15, dynamin2, pDG and pTRUF12 plasmids, respectively. We thank Harvey T. MacMahon (Medical Research Council, Cambridge, UK) for the GRAF1 antibody and Kleopatra Rapti and Lifan Liang (Mount Sinai School of Medicine, New York, NY) for Ad5 vectors. We are grateful to Serine Avagyan, Lorenzo Battini and Raphael Rozenfeld (Mount Sinai School

of Medicine, New York NY) for their help with flow cytometry and microscopy, and Christophe Lamaze (Institut Curie, Paris, France) for helpful discussions and advice. We thank Ronald Gordon and Heather Bell from the Pathology Core Electron Microscopy Facility of the Mount Sinai School of Medicine (New York, NY) for their help. We gratefully acknowledge the continuous support by Roger, J. Hajjar (Mount Sinai School of Medicine, New York, NY; R.J.H.). This work was supported by US National Institutes of Health Grants HL077322 (to T.W.), and HL100396 and HL088434 (to R.J.H.).

References

Bartlett JS, Wilcher R, Samulski RJ. Infectious entry pathway of adeno-associated virus and adeno-associated virus vectors. J Virol. 2000; 74:2777–2785. [PubMed: 10684294]

Benmerah A, Bayrou M, Cerf-Bensussan N, Dautry-Varsat A. Inhibition of clathrin-coated pit assembly by an Eps15 mutant. J Cell Sci. 1999; 112(Pt 9):1303–1311. [PubMed: 10194409]

Bhrigu V, Trempe JP. Adeno-associated virus infection of murine fibroblasts with help provided by mouse adenovirus. Virology. 2009; 390:22–30. [PubMed: 19464040]

Chadda R, Howes MT, Plowman SJ, Hancock JF, Parton RG, Mayor S. Cholesterol-sensitive Cdc42 activation regulates actin polymerization for endocytosis via the GEEC pathway. Traffic. 2007; 8:702–717. [PubMed: 17461795]

Cortese K, Sahores M, Madsen CD, Tacchetti C, Blasi F. Clathrin and LRP-1-independent constitutive endocytosis and recycling of uPAR. PLoS One. 2008; 3:e3730. [PubMed: 19008962]

Damm EM, Pelkmans L, Kartenbeck J, Mezzacasa A, Kurzchalia T, Helenius A. Clathrin- and caveolin-1-independent endocytosis: entry of simian virus 40 into cells devoid of caveolae. J Cell Biol. 2005; 168:477–488. [PubMed: 15668298]

Daya S, Berns KI. Gene therapy using adeno-associated virus vectors. Clin Microbiol Rev. 2008; 21:583–593. [PubMed: 18854481]

Doherty GJ, Lundmark R. GRAF1-dependent endocytosis. Biochem Soc Trans. 2009; 37:1061–1065. [PubMed: 19754452]

Doherty GJ, McMahon HT. Mechanisms of endocytosis. Annu Rev Biochem. 2009; 78:857–902. [PubMed: 19317650]

Douar AM, Poulard K, Stockholm D, Danos O. Intracellular trafficking of adeno-associated virus vectors: routing to the late endosomal compartment and proteasome degradation. J Virol. 2001; 75:1824–1833. [PubMed: 11160681]

Duan D, Li Q, Kao AW, Yue Y, Pessin JE, Engelhardt JF. Dynamin is required for recombinant adeno-associated virus type 2 infection. J Virol. 1999; 73:10371–10376. [PubMed: 10559355]

Ewers H, Romer W, Smith AE, Bacia K, Dmitrieff S, Chai W, Mancini R, Kartenbeck J, Chambon V, Berland L, et al. GM1 structure determines SV40-induced membrane invagination and infection. Nat Cell Biol. 2009; 12:11–18. 11–12. [PubMed: 20023649]

Ferrari FK, Samulski T, Shenk T, Samulski RJ. Second-strand synthesis is a rate-limiting step for efficient transduction by recombinant adeno-associated virus vectors. J Virol. 1996; 70:3227–3234. [PubMed: 8627803]

Gigout L, Rebollo P, Clement N, Warrington KH Jr, Muzyczka N, Linden RM, Weber T. Altering AAV tropism with mosaic viral capsids. Mol Ther. 2005; 11:856–865. [PubMed: 15922956]

Grimm D, Kay MA. From virus evolution to vector revolution: use of naturally occurring serotypes of adeno-associated virus (AAV) as novel vectors for human gene therapy. Curr Gene Ther. 2003; 3:281–304. [PubMed: 12871018]

Grimm D, Kern A, Rittner K, Kleinschmidt JA. Novel tools for production and purification of recombinant adenoassociated virus vectors. Hum Gene Ther. 1998; 9:2745–2760. [PubMed: 9874273]

Hansen J, Qing K, Kwon HJ, Mah C, Srivastava A. Impaired intracellular trafficking of adeno-associated virus type 2 vectors limits efficient transduction of murine fibroblasts. J Virol. 2000; 74:992–996. [PubMed: 10623762]

Hirosue S, Senn K, Clement N, Nonnenmacher M, Gigout L, Linden RM, Weber T. Effect of inhibition of dynein function and microtubule-altering drugs on AAV2 transduction. Virology. 2007; 367:10–18. [PubMed: 17588632]

Howes MT, Kirkham M, Riches J, Cortese K, Walser PJ, Simpson F, Hill MM, Jones A, Lundmark R, Lindsay MR, et al. Clathrin-independent carriers form a high capacity endocytic sorting system at the leading edge of migrating cells. J Cell Biol. 2010; 190:675–691. [PubMed: 20713605]

Johnson J, Li C, Diprimio N, Weinberg M, McCown T, Samulski R. Mutagenesis of adeno-associated virus type 2 capsid protein VP1 uncovers new roles for basic amino acids in trafficking and cell-specific transduction. J Virol. 2010; 84:8888–8902. [PubMed: 20573820]

Kalia M, Kumari S, Chadda R, Hill MM, Parton RG, Mayor S. Arf6-independent GPI-anchored protein-enriched early endosomal compartments fuse with sorting endosomes via a Rab5/phosphatidylinositol-3′-kinase-dependent machinery. Mol Biol Cell. 2006; 17:3689–3704. [PubMed: 16760436]

Kirkham M, Fujita A, Chadda R, Nixon SJ, Kurzchalia TV, Sharma DK, Pagano RE, Hancock JF, Mayor S, Parton RG. Ultrastructural identification of uncoated caveolin-independent early endocytic vehicles. J Cell Biol. 2005; 168:465–476. [PubMed: 15668297]

Koivusalo M, Welch C, Hayashi H, Scott CC, Kim M, Alexander T, Touret N, Hahn KM, Grinstein S. Amiloride inhibits macropinocytosis by lowering submembranous pH and preventing Rac1 and Cdc42 signaling. J Cell Biol. 2010; 188:547–563. [PubMed: 20156964]

Kumari S, Mayor S. ARF1 is directly involved in dynamin-independent endocytosis. Nat Cell Biol. 2008; 10:30–41. [PubMed: 18084285]

Lakhan SE, Sabharanjak S, De A. Endocytosis of glycosylphosphatidylinositol-anchored proteins. J Biomed Sci. 2009; 16:93. [PubMed: 19832981]

Legler DF, Doucey MA, Schneider P, Chapatte L, Bender FC, Bron C. Differential insertion of GPI-anchored GFPs into lipid rafts of live cells. Faseb J. 2005; 19:73–75. [PubMed: 15516372]

Lundmark R, Doherty GJ, Howes MT, Cortese K, Vallis Y, Parton RG, McMahon HT. The GTPase-activating protein GRAF1 regulates the CLIC/GEEC endocytic pathway. Curr Biol. 2008; 18:1802–1808. [PubMed: 19036340]

Macia E, Ehrlich M, Massol R, Boucrot E, Brunner C, Kirchhausen T. Dynasore, a cell-permeable inhibitor of dynamin. Dev Cell. 2006; 10:839–850. [PubMed: 16740485]

Meier O, Greber UF. Adenovirus endocytosis. J Gene Med. 2003; 5:451–462. [PubMed: 12797110]

Mercer J, Helenius A. Virus entry by macropinocytosis. Nat Cell Biol. 2009; 11:510–520. [PubMed: 19404330]

Mercer J, Schelhaas M, Helenius A. Virus entry by endocytosis. Annu Rev Biochem. 2010; 79:803–833. [PubMed: 20196649]

Nichols BJ. A distinct class of endosome mediates clathrin-independent endocytosis to the Golgi complex. Nat Cell Biol. 2002; 4:374–378. [PubMed: 11951093]

Nichols BJ, Kenworthy AK, Polishchuk RS, Lodge R, Roberts TH, Hirschberg K, Phair RD, Lippincott-Schwartz J. Rapid cycling of lipid raft markers between the cell surface and Golgi complex. J Cell Biol. 2001; 153:529–541. [PubMed: 11331304]

Pajusola K, Gruchala M, Joch H, Luscher TF, Yla-Herttuala S, Bueler H. Cell-type-specific characteristics modulate the transduction efficiency of adeno-associated virus type 2 and restrain infection of endothelial cells. J Virol. 2002; 76:11530–11540. [PubMed: 12388714]

Parton RG, Joggerst B, Simons K. Regulated internalization of caveolae. J Cell Biol. 1994; 127:1199–1215. [PubMed: 7962085]

Pelkmans L, Kartenbeck J, Helenius A. Caveolar endocytosis of simian virus 40 reveals a new two-step vesicular-transport pathway to the ER. Nat Cell Biol. 2001; 3:473–483. [PubMed: 11331875]

Ren C, White AF, Ponnazhagan S. Notch1 augments intracellular trafficking of adeno-associated virus type 2. J Virol. 2007; 81:2069–2073. [PubMed: 17151095]

Ridley AJ, Hall A. The small GTP-binding protein rho regulates the assembly of focal adhesions and actin stress fibers in response to growth factors. Cell. 1992; 70:389–399. [PubMed: 1643657]

Sabharanjak S, Sharma P, Parton RG, Mayor S. GPI-anchored proteins are delivered to recycling endosomes via a distinct cdc42-regulated, clathrin-independent pinocytic pathway. Dev Cell. 2002; 2:411–423. [PubMed: 11970892]

Sanlioglu S, Benson PK, Yang J, Atkinson EM, Reynolds T, Engelhardt JF. Endocytosis and nuclear trafficking of adeno-associated virus type 2 are controlled by rac1 and phosphatidylinositol-3 kinase activation. J Virol. 2000; 74:9184–9196. [PubMed: 10982365]

Sieczkarski SB, Whittaker GR. Dissecting virus entry via endocytosis. J Gen Virol. 2002; 83:1535–1545. [PubMed: 12075072]

Swanson JA. Phorbol esters stimulate macropinocytosis and solute flow through macrophages. J Cell Sci. 1989; 94(Pt 1):135–142. [PubMed: 2613767]

Tkachenko E, Lutgens E, Stan RV, Simons M. Fibroblast growth factor 2 endocytosis in endothelial cells proceed via syndecan-4-dependent activation of Rac1 and a Cdc42-dependent macropinocytic pathway. J Cell Sci. 2004; 117:3189–3199. [PubMed: 15226395]

Wallen AJ, Barker GA, Fein DE, Jing H, Diamond SL. Enhancers of adeno-associated virus AAV2 transduction via high throughput siRNA screening. Mol Ther. 2011; 19:1152–1160. [PubMed: 21304495]

Wang LH, Rothberg KG, Anderson RG. Mis-assembly of clathrin lattices on endosomes reveals a regulatory switch for coated pit formation. J Cell Biol. 1993; 123:1107–1117. [PubMed: 8245121]

Wang Z, Ma HI, Li J, Sun L, Zhang J, Xiao X. Rapid and highly efficient transduction by double-stranded adeno-associated virus vectors in vitro and in vivo. Gene Ther. 2003; 10:2105–2111. [PubMed: 14625564]

Xiao W, Warrington KH Jr, Hearing P, Hughes J, Muzyczka N. Adenovirus-facilitated nuclear translocation of adeno-associated virus type 2. J Virol. 2002; 76:11505–11517. [PubMed: 12388712]

Zolotukhin S, Byrne BJ, Mason E, Zolotukhin I, Potter M, Chesnut K, Summerford C, Samulski RJ, Muzyczka N. Recombinant adeno-associated virus purification using novel methods improves infectious titer and yield. Gene Ther. 1999; 6:973–985. [PubMed: 10455399]

HIGHLIGHTS

- AAV2 infection is independent of clathrin, caveolin, dynamin or macropinocytosis
- AAV2 infection is dependent on actin and cholesterol
- The infectious entry of AAV2 proceeds through clathrin-independent carriers (CLIC)
- AAV2 is internalized in GPI-anchored-protein-enriched endosomal compartments (GEECs)

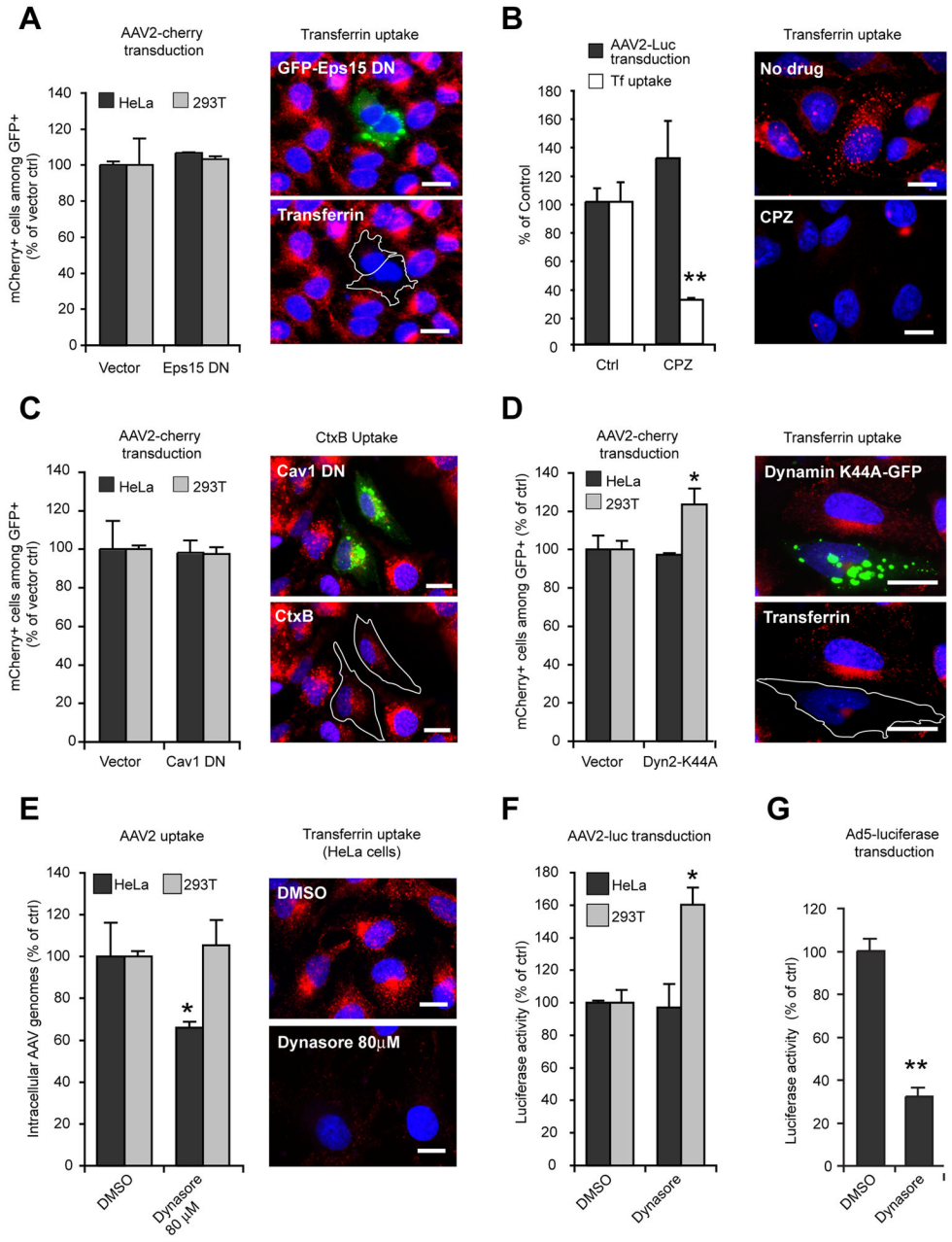

Figure 1. AAV2 Transduction Is Clathrin- Caveolin- and Dynamin-Independent

(A) Left panel: AAV2-cherry transduction of HeLa and 293T cells transfected with EGFP-Eps15Δ95/295, as analyzed by flow cytometry. Transfected cells (GFP+) were gated, and the fraction of transduced cells among transfected cells (GFP+/mCherry+) was measured. Values are normalized to vector-transfected cells. Right panel: HeLa cells transfected with EGFP-Eps15Δ95/295 (green) were exposed to fluorescent transferrin (red) for 15 min and observed by wide-field fluorescent microscopy with a 63X objective. Transfected cells are outlined in white. Bar, 10 μm.

(B) HeLa cells were infected with AAV2-luc in the presence or absence of chlorpromazine (CPZ, 20 μM). Luciferase activity (black bars) was normalized to untreated control cells.

Fluorescent transferrin uptake (white bars and right panels) was quantified by microscopy image analysis as described in Experimental Procedures.
(C) AAV2 transduction (left) and uptake of cholera toxin B (right; CtxB, red) by HeLa cells expressing dominant negative EGFP-caveolin1 (Cav1DN, green). Cells were exposed to Alexa555-cholera toxinB (CtxB) for 1 hr. Bar, 10 μm.
(D) Flow cytometry analysis of AAV2-cherry transduction of HeLa and 293T cells transfected with EGFP-Dyn2K44A mutant. Analysis was performed as described in Fig. 1A. Right panel: transferrin uptake (red) in HeLa cells transfected with EGFP-Dyn2K44A (green).
(E) AAV2-Luc uptake in HeLa and 293T cells treated with 80 μM dynasore. Viral DNA was quantified by qPCR. Values are normalized to DMSO-treated control cells. Right panels, transferrin uptake in HeLa cells treated with 80 μM dynasore. Bar, 10 μm.
(F) AAV2-luc transduction of HeLa and 293T cells treated with 80 μM dynasore. Luciferase values were normalized to DMSO-treated control cells.
(G) Adenovirus type 5 – luciferase (Ad5-luc) transduction of HeLa cells in the presence of 80 μM dynasore. Luciferase values were normalized to DMSO-treated control cells.
Error bars indicate SD, *$p < 0.05$, **$p < 0.005$. Because the values are normalized to control cells, values in this and other figures can exceed 100%.

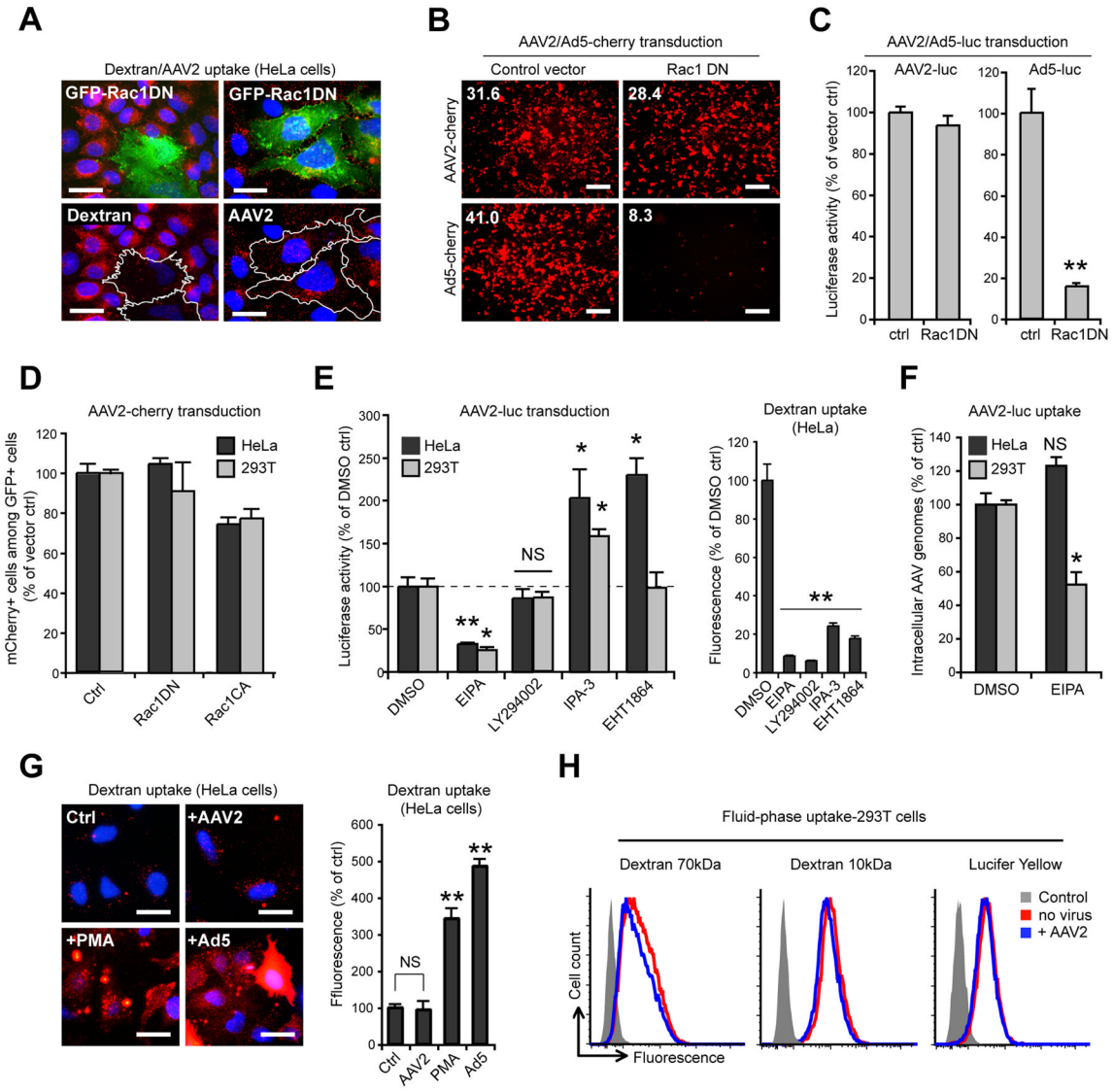

Figure 2. AAV2 Transduction Does Not Involve Macropinocytosis

(A) HeLa cells expressing EGFP-tagged dominant negative Rac1 (Rac1DN, green) were assayed for 70 kDa dextran or AAV2 (red) endocytosis. Transfected cells are outlined in white. Bar, 10 μm.

(B) AAV2-cherry and Ad5-cherry transduction of 293T cells expressing EGFP-Rac1DN. Transfection efficiency was approximately 90% (not shown). Low-magnification micrographs were acquired with a 5X objective. Values indicate mean red fluorescence intensity per microscope field. Bar, 100 μm.

(C) AAV2-luc and Ad5-luc transduction of 293T cells expressing EGFP-Rac1DN. Values are normalized to EGFP vector controls.

(D) Flow cytometry analysis of AAV2-cherry transduction in HeLa and 293T cells expressing EGFP-Rac1DN or EGFP-Rac1CA (constitutively active). Values are normalized to EGFP-expressing controls.

(E) AAV2-luc transduction (left panel) and fluorescent 70 kDa dextran internalization (right panel) in cells treated with EIPA (a fluid-phase endocytosis inhibitor), LY294002 (a PI3K inhibitor), IPA-3 (a PAK1 inhibitor) or EHT1864 (a Rac1 inhibitor).

(F) AAV2-luc uptake in cells treated with EIPA. Values are normalized to DMSO-treated cells.
(G) Dextran uptake in HeLa cells incubated with AAV2-luc (10^5 gcp/cell), PMA (1 μM) or Ad5 (10^5 gcp/cell). Mean fluorescence values are normalized to DMSO-treated control. Bar, 10 μm.
(H) Flow cytometry analysis of 293T cells incubated for 30min with fluorescent 70 kDa dextran, 10 kDa dextran or lucifer yellow (LY) in the absence or presence of AAV2-luc (10^5 gcp/cell).
Error bars indicate SD, *$p < 0.05$, **$p < 0.005$. NS, Not Significant.

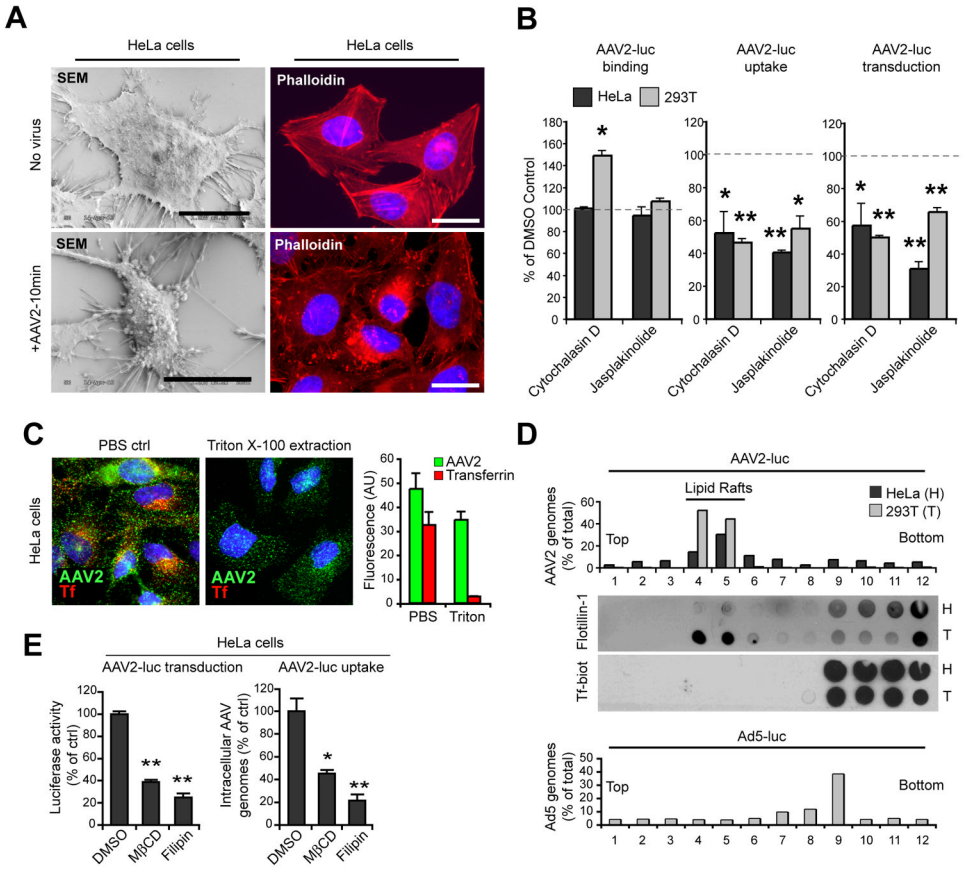

Figure 3. AAV2 Entry and Transduction Involve Actin Cytoskeleton and Membrane Cholesterol

(A) Surface morphology and actin remodeling of HeLa cells exposed to AAV2-luc (10^5 gcp/cell, lower panels) or mock-treated (upper panels) for 1hr on ice and then transferred to 37 °C for 10 min. Cells were visualized by scanning electron microscopy (SEM, left panels). Actin cytoskeleton was observed by phalloidin staining (right panels). Bar, 10 μm.

(B) AAV2 binding, uptake and transduction in HeLa and 293T cells treated with cytochalasin D or jasplakinolide. Values are normalized to DMSO-treated control cells (represented by dashed lines).

(C) Resistance of AAV2 to triton extraction. HeLa cells incubated with fluorescent transferrin and AAV2-luc for 30 min were subjected to triton X-100 extraction and stained for AAV2 capsids. Right panel: quantification of red (transferrin) and green (AAV2) fluorescence (arbitrary units) was performed from three independent samples.

(D) Sucrose density fractionation of Triton X-100 extracts from HeLa (H) and 293T (T) cells incubated with AAV2 and biotin-transferrin for 30 min ar 37 °C. Viral DNA recovered from each fraction was quantified by qPCR. Endogenous flotillin1 was detected by dot blot from the same fractions. Control Ad5-luc fractionation (lower panel) was obtained from a separate sample of 293T cells.

(E) AAV2-luc transduction and endocytosis in HeLa cells treated with methyl-β-cyclodextrin or filipin III. Values are normalized to DMSO-treated control cells.

Error bars indicate SD, *$p < 0.05$, **$p < 0.005$.

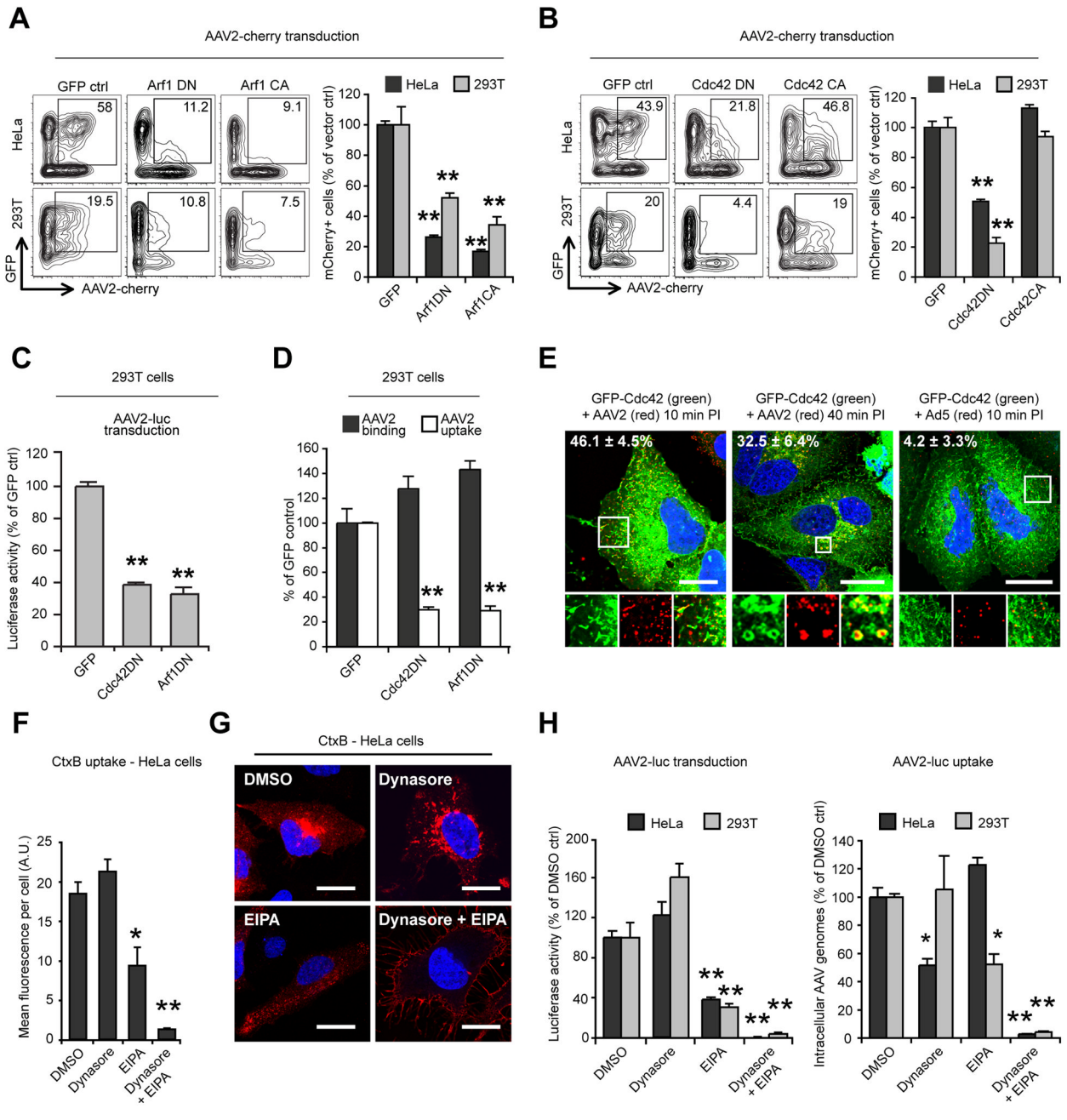

Figure 4. AAV2 Infection Requires Arf1 and Cdc42

(A) AAV2-cherry transduction of HeLa and 293T cells expressing EGFP-tagged Arf1 dominant-negative (DN) and constitutively active (CA) mutants. Flow cytometry analysis was performed as described in Figure 1A. Insets represent the selected EGFP+/mCherry+ populations, and numbers indicate the percentage of mCherry+ cells among the EGFP+ population.

(B) AAV2-cherry transduction of HeLa and 293T cells expressing EGFP-tagged Cdc42 DN and CA mutants; analysis as described above.

(C) AAV2-luc transduction of 293T cells expressing dominant-negative Arf1 or Cdc42. Values are normalized to GFP vector-transfected controls.

(D) AAV2 binding and endocytosis in 293T cells transfected with dominant-negative Arf1 or Cdc42. Transfection efficiency was approximately 80% (not shown).
(E) Co-localization of Cdc42 with AAV2 or Ad5 in HeLa cells. Cells were transfected with EGFP-Cdc42WT, infected with AAV2-luc or Ad5-luc and stained for AAV2 or Ad5 capsids. Insets show higher magnification of boxed areas. Values indicate the percentage of virus (red) overlapping with Cdc42 (green). Bar, 20 μm.
(F) CtxB internalization (30 min) in HeLa cells treated with 100 μM EIPA, 80μM dynasore, or both. Surface-bound CtxB was removed by acid-stripping for intracellular fluorescence quantification.
(G) Confocal micrographs of HeLa cells treated as above. Acid wash was omitted to show surface accumulation of CtxB in cells treated with dynasore and EIPA. Bar, 10 μM.
(H) Synergistic effect of EIPA and dynasore on AAV2-luc transduction (left panel) and internalization (right panel). Values are normalized to DMSO controls.
Error bars indicate SD, *$p < 0.05$, **$p < 0.005$.

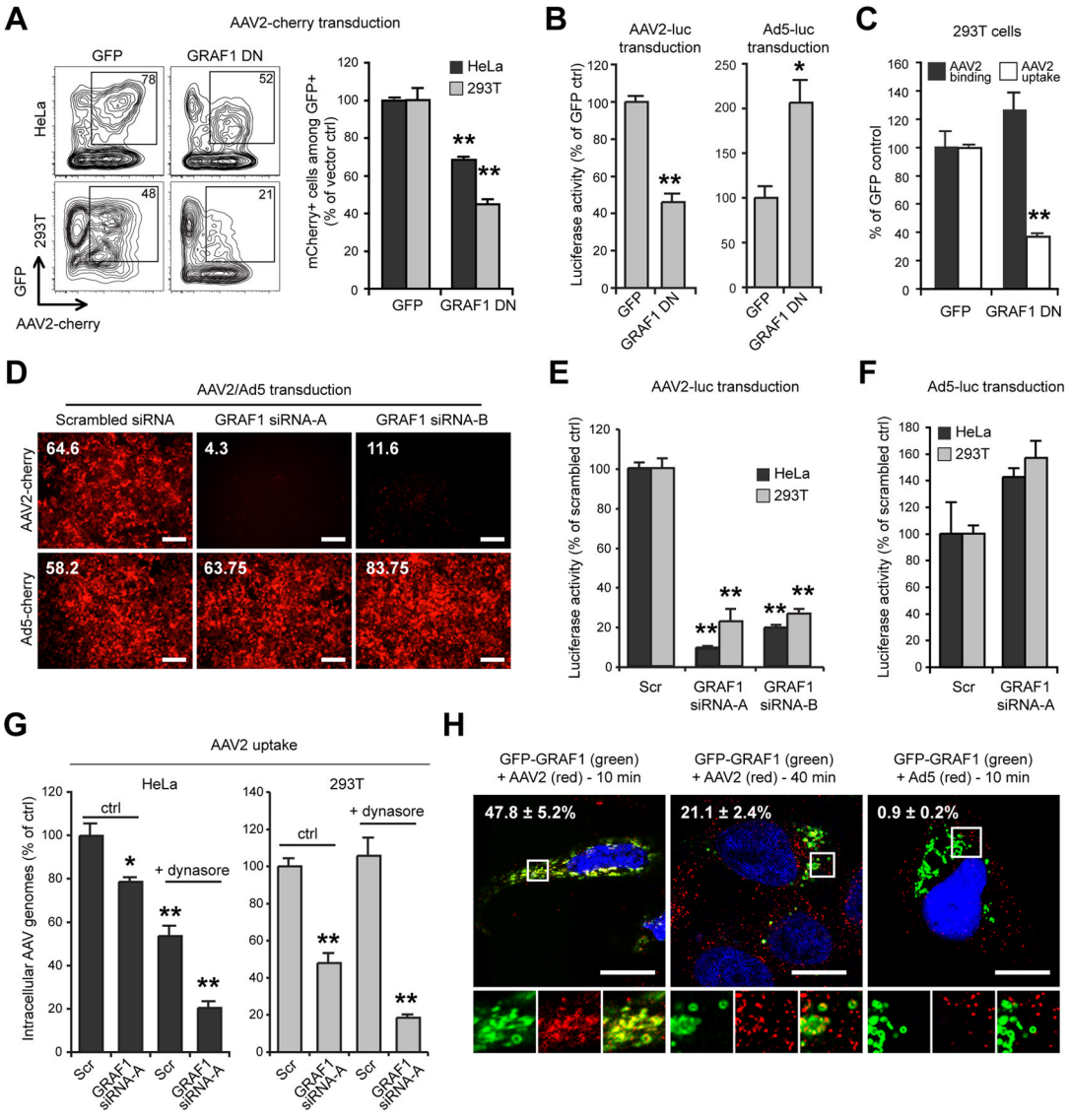

Figure 5. AAV2 Infection is GRAF1-Dependent

(A) Transduction of HeLa and 293T cells expressing EGFP-tagged dominant negative GRAF1. Flow cytometry analysis was performed as described in Figure 1A and 4A.

(B) AAV2-luc and Ad5-luc transduction of 293T cells expressing GFP-GRAF1DN. Values are normalized to EGFP vector control.

(C) Binding and endocytosis of AAV2 in 293T cells expressing GFP-GRAF1DN. Values are normalized to EGFP vector control.

(D) AAV2-cherry and Ad5-cherry transduction of 293T cells following GRAF1 knockdown by siRNA. Numbers indicate mean red fluorescence of pictured low-magnification microscope fields. Similar results were obtained with HeLa cells (not shown). Bar, 100 μm.

(E) AAV2-luc and (F) Ad5-luc transduction of HeLa and 293T cells following GRAF1 knock-down by siRNA A or B. Values are normalized to scrambled siRNA controls (scr).

(G) AAV2-luc endocytosis in HeLa and 293T cells transfected with GRAF1 siRNA with or without dynasore treatment. Values are normalized to scrambled siRNA/DMSO controls.

(H) Confocal microscopy localization of GFP-GRAF1 (green) with AAV2 or Ad5 virions (red) in HeLa cells. Insets show higher magnifications of boxed areas. Values indicate the percentage of virus (red) overlapping with GRAF1 (green). Bar, 10 μm.
Error bars indicate SD, *$p < 0.05$, **$p < 0.005$.

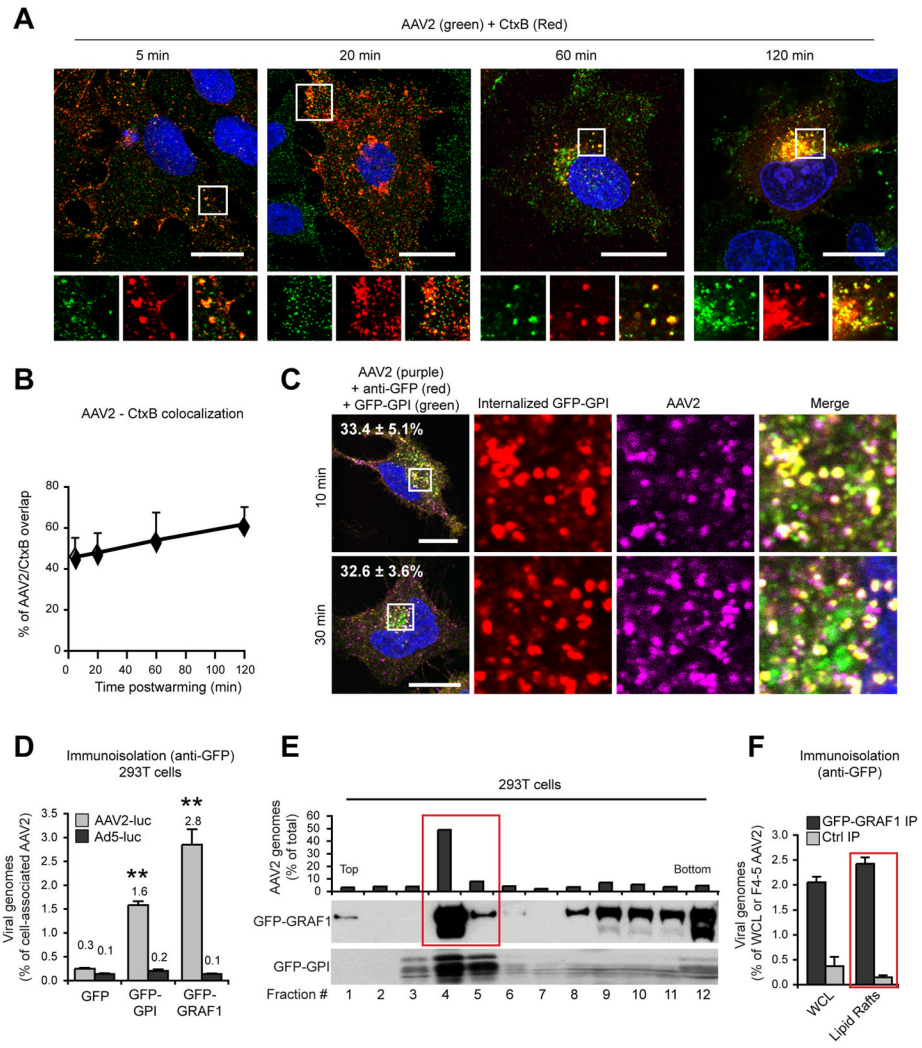

Figure 6. Co-Localization of AAV2 with Cholera Toxin B and GFP-GPI

(A) Confocal microscopy localization of AAV2 (green) with fluorescent Cholera toxin B (red). Insets show higher magnifications of boxed areas.

(B) Quantification of AAV2/CtxB co-localization in A. Values indicate the percentage of AAV2 (green) overlapping with CtxB (red).

(C) HeLa cells transfected with GFP-GPI (green), were incubated 30 min on ice with AAV2 (purple) and Alexa 555-conjugated anti-GFP polyclonal antibody (red), washed and transferred to 37 °C for the indicated times. After removal of surface labeling by PI-PLC and heparin, internalized AAV2 capsids were stained with A20 followed by a Cy5 secondary antibody. Insets show higher magnifications of boxed areas. Values show the percentage of AAV2 (purple) overlapping with internalized anti-GFP antibody (red). Bar, 10 μm.

(D) Quantification of AAV2 or Ad5 genomes in GPI- or GRAF1-enriched vesicles purified by immunoisolation. 293T cells transfected with GFP-tagged GPI or GRAF1 were infected with AAV2-luc or Ad5-luc (10^4 gcp/cell) and whole cell lysates were immunoprecipitated with an anti-GFP antibody as described in Experimental Procedures. AAV2 and Ad5 DNA recovered from immunoisolates were quantified by qPCR. Values are normalized to the total viral DNA in each cell lysate.

(E) Sucrose density fractionation of GFP-GRAF1 and GFP-GPI in transfected 293T cells. GFP-GPI fractions were obtained from a different sample. The fractions 4 and 5 (boxed) were used for the immunoisolation experiments in F.
(F) Immunoisolation of GRAF1-enriched endosomal vesicles from lipid rafts. Immunoprecipitations were performed from whole cell lysate (WCL) or pooled lipid raft fractions 4 and 5 (highlighted in red) with an anti-GFP antibody (GRAF1 IP) or with normal mouse serum as a negative control (ctrl IP). Viral genomes present in the immunoprecipitates were quantified by qPCR. Values were normalized to the total amount of viral DNA in the whole lysate or in the pooled fractions 4 and 5.
Error bars indicate SD, $^{**}p < 0.005$.

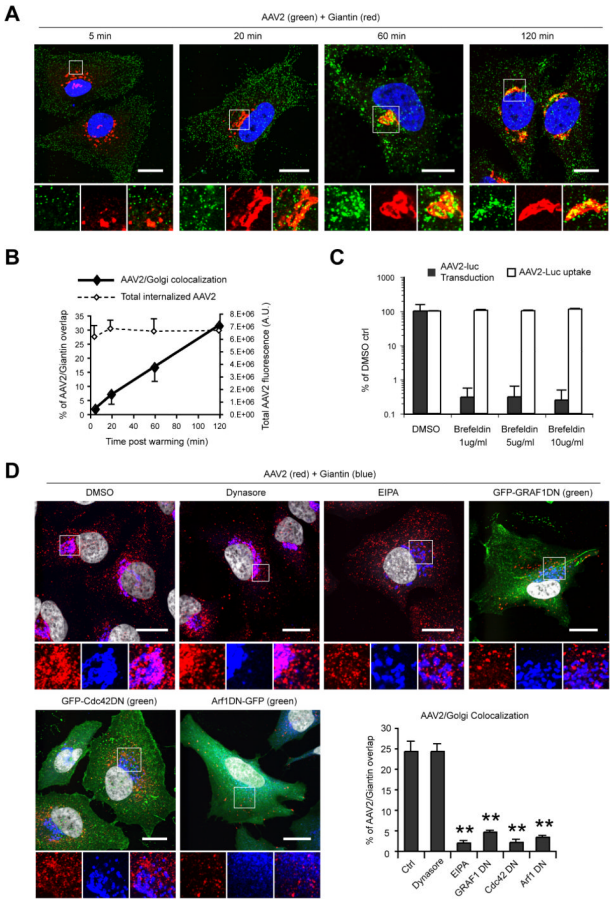

Figure 7. Post-Entry Trafficking of AAV2

(A) Confocal microscopy localization of AAV2 (green) and the Golgi marker giantin (red). Insets show higher magnifications of boxed areas. Bar, 20 μm.

(B) Quantification of AAV2/Golgi co-localization. Values indicate the percentage of AAV2 (green) overlapping with Giantin (red). Mean fluorescence intensity of total internalized AAV2 is shown as dotted line.

(C) AAV2 transduction and uptake in HeLa cells treated with brefeldin A (BFA). Values are normalized to DMSO ctrls.

(D) Confocal microscopy localization of AAV2 (red) and Golgi (anti-giantin, Cy5 pseudocolored in blue) in HeLa cells treated with dynasore, EIPA, or transfected with dominant-negative GRAF1, Cdc42 or Arf1 (green). Values in the graph indicate the percentage of AAV2 (red) overlapping with giantin (blue). Nuclei were stained with DAPI and pseudocolored in grayscale. Bar, 10 μm.

Error bars indicate SD, **p < 0.005.